Title

Anisotropy of Bullet-Shaped Magnetite Nanoparticles in the Magnetotactic Bacteria Desulfovibrio magneticus sp. Strain RS-1

Journal

Biophysical Journal, 108(5)

ISSN

0006-3495

Authors

Chariaou, Michalis
Rahn-Lee, Lilah
Kind, Jessica
et al.

Publication Date

2015-03-01

DOI

10.1016/j.bpj.2015.01.007

Peer reviewed

Article

Anisotropy of Bullet-Shaped Magnetite Nanoparticles in the Magnetotactic Bacteria *Desulfovibrio magneticus sp.* Strain RS-1

Michalis Chariaou,[1] Lilah Rahn-Lee,[2] Jessica Kind,[3] Inés García-Rubio,[4,5] Arash Komeili,[2] and Andreas U. Gehring[3,*]

[1]Department of Physics and [2]Plant and Microbial Biology, University of California, Berkeley, California; [3]Institute of Geophysics and [4]Laboratory of Physical Chemistry, ETH Zurich, Zurich, Switzerland; and [5]Centro Universitario de la Defensa, Zaragoza, Spain

ABSTRACT Magnetotactic bacteria (MTB) build magnetic nanoparticles in chain configuration to generate a permanent dipole in their cells as a tool to sense the Earth's magnetic field for navigation toward favorable habitats. The majority of known MTB align their nanoparticles along the magnetic easy axes so that the directions of the uniaxial symmetry and of the magnetocrystalline anisotropy coincide. *Desulfovibrio magneticus sp.* strain RS-1 forms bullet-shaped magnetite nanoparticles aligned along their (100) magnetocrystalline hard axis, a configuration energetically unfavorable for formation of strong dipoles. We used ferromagnetic resonance spectroscopy to quantitatively determine the magnetocrystalline and uniaxial anisotropy fields of the magnetic assemblies as indicators for a cellular dipole with stable direction in strain RS-1. Experimental and simulated ferromagnetic resonance spectral data indicate that the negative effect of the configuration is balanced by the bullet-shaped morphology of the nanoparticles, which generates a pronounced uniaxial anisotropy field in each magnetosome. The quantitative comparison with anisotropy fields of *Magnetospirillum gryphiswaldense*, a model MTB with equidimensional magnetite particles aligned along their (111) magnetic easy axes in well-organized chain assemblies, shows that the effectiveness of the dipole is similar to that in RS-1. From a physical perspective, this could be a reason for the persistency of bullet-shaped magnetosomes during the evolutionary development of magnetotaxis in MTB.

INTRODUCTION

Magnetotactic bacteria (MTB) are a classical example of microbes that have developed a sensor for magnetic fields (1). The MTB are a diverse group of strains that generate magnetic dipoles in their cells by precipitation and arrangement of ferrimagnetic nanoparticles into chains (2–6). They live motile in aquatic systems and it is assumed that the nanoparticle assemblies generate a magnetic dipole, which acts as a compass for navigation along the Earth's magnetic field toward favorable habitats, a process denoted magnetotaxis. It is well established that the formation of magnetic nanoparticles by MTB in membrane-bound organelles known as magnetosomes is a genetically controlled process. Specific biomineralization proteins are indispensable for the formation of the magnetosomes, i.e., the chemical composition, size, shape, and organization of the nanocrystals (7–12). Genetically encoded nanoparticles exhibit little morphological variation within each strain and consist of the ferrimagnetic mineral magnetite (Fe_3O_4) or, to a lesser extent, greigite (Fe_3S_4) in a stable single-domain range between 30 and 100 nm (13,14). The comparison between different MTB strains has shown prominent variations in the shape and organization of the nanoparticles (4,12).

Recent genome sequencing has revealed that all known MTB strains can be affiliated with the α-, γ-, and δ-proteobacteria classes of the Proteobacteria phylum, or the Nitrospirae phylum and OP3 division (4). Magnetite nanoparticles occur in all four taxa. In species of the α- and γ-proteobacteria, the magnetite nanoparticles are uniform, have cuboctahedral or elongated prismatic morphologies, and are organized in chain configurations with aligned (111) magnetic easy axes, i.e., in energetically favorable directions for spontaneous magnetization. In contrast, species of the δ-proteobacteria and Nitrospirae phylum show elongated bullet-shaped nanoparticles, which are aligned along the (100) magnetocrystalline hard axes in relatively loose chain configurations compared to those in α-proteobacteria (15–17). It has been argued that there is a link between the morphology and organization of the nanoparticles and the phylogenetic affiliation (see, e.g., Pósfai et al. (12)). Based on phylogenetic considerations, Lefèvre et al. (4) have suggested that the earliest magnetic constituents in MTB were elongated-anisotropic magnetite nanoparticles, similar to those found in δ-proteobactertia. Given that all MTB generate a magnetic dipole, a quantitative comparison of the anisotropy properties of the cellular magnetosomes in α- and δ-proteobacteria can be used to infer changes in the dipole stability and in turn the effectiveness of magnetotaxis during evolution.

Ferromagnetic resonance spectroscopy (FMR) is a powerful tool for analyzing the anisotropy of magnetic

Submitted September 29, 2014, and accepted for publication January 5, 2015.

*Correspondence: agehring@erdw.ethz.ch

Editor: Charles Wolgemuth.

0006-3495/15/03/1268/7 $2.00

http://dx.doi.org/10.1016/j.bpj.2015.01.007

materials, and it has been applied to the study of MTB (18–22). Thus far, quantitative FMR analyses have been reported for cultured species of the α-proteobacteria class, such as *Magnetospirrilum gryphiswaldense* MRS-1 (23,24). It has been shown that the uniaxial anisotropy field (H_{uni}) due to the magnetosome organization in intact chains exceeds the magnetocrystalline field (H_{cub}) yielded by individual magnetite nanoparticles, $|H_{uni}/H_{cub}| >> 1$ (25), i.e., the configuration of the magnetosomes in the cell is essential for the magnetotaxis of MTB.

There are no reports on the strength of the anisotropy fields in MTB that are generated by irregular bullet-shaped magnetosomes with less organized chain configuration. Among these MTB species, *Desulfovibrio magneticus sp.* RS-1 (RS-1) of the δ-proteobacteria class is an ideal candidate to study the anisotropy properties because it is a cultured MTB outside the α-proteobacteria that forms bullet-shaped nanoparticles (26). A morphological and magnetic study of cultured RS-1 by Pósfai et al. (15) showed that MTB cells contain (100) elongated single-domain and smaller superparamagnetic magnetite particles in a not-well-organized chain configuration, which results in weak magnetotaxis. In addition to the intracellular particles, RS-1 cells exhibit hematite nanoparticles on the surface, which is interpreted as biologically induced mineralization. The (100) alignment of elongated magnetic particles in the RS-1 cell as a configuration to generate magnetotaxis has been confirmed by synchrotron x-ray diffraction (16). Moreover, the authors of that study report that the magnetic hard axis in magnetite can be turned into an effective easy axis by particle elongation along (100) for aspect ratios exceeding 1.25.

The aim of this article is to present a quantitative FMR analysis of cultured RS-1 as a requirement for the comparison of the anisotropy properties in MTB of different Proteobacteria classes to resolve whether anisotropy properties of different magnetosome configurations indicate an evolutionary trend in optimization of magnetotaxis. We will show by comparing strains RS-1 and MRS-1 that despite the fundamental differences in the formation and organization of magnetic nanoparticles within the diverse groups of MTB, the magnetic dipole is preserved and uniaxial anisotropy fields are still dominant in the chain, even when the intracellular configuration of magnetosomes changes drastically.

MATERIALS AND METHODS

Sample preparation

Cultures of RS-1 strain were grown as previously reported (27), except that 25 mM 4-(2-hydroxyethyl)-1-piper-azineethanesulfonic acid was added to the growth media and the pH was set to 6.7. Samples were collected at early stationary phase. The microstructure of the MTB was investigated by means of transmission electron microscopy (TEM), as described in Byrne et al. (27). Based on TEM micrographs, statistics of the particle sizes ($n = 433$) in RS-1 was performed. To broaden the statistical basis, bacteria from four experimental series were used. For experiments involving fixed cells, the RS-1 cell pellet was washed once in PBS and then fixed with 2.5% gluteraldehyde.

FMR experiments

For the quantification of the magnetic anisotropy in MTB, we used FMR spectroscopy, which is a powerful technique for measuring anisotropy fields related to the shape of the particle and the arrangement of the set of particles (23,28). In FMR experiments, the precessional motion (Larmor precession) of the magnetization in an external magnetic field is enhanced by a perpendicularly incoming microwave field when the microwave frequency matches the Larmor frequency of the system (resonance). Hence, in a field-sweep experiment, microwave absorption occurs when the Larmor frequency of the magnetic moments coincides with the microwave frequency (see, e.g., Vonsovskii (18)). The X-band spectra were recorded on an E500 spectrometer from Bruker biospin working at a microwave frequency of 9.81 GHz, with a microwave power of 0.06 mW. The applied magnetic field was modulated with a frequency of 100 kHz and modulation amplitude of 1 Oe (80 A/m). The spectrometer was equipped with a goniometer and a nitrogen gas-flow cryostat (21,24).

The anisotropy properties of the RS-1 strain were investigated on randomly distributed (bulk) and oriented (the individual MTB chains are parallel to each other) bacterial samples from the same experimental series. In the former case, the lyophilized culture of MTB was put in an electron spin resonance (ESR) quartz glass tube 4 mm in diameter and then fixed in a paraffin matrix to avoid its alignment in an external magnetic field during the FMR experiment. For the measurement on oriented samples, an ESR glass tube was filled with 100 μL of MTB aqueous suspension together with 50 μL of glycerol. For alignment of the MTB, the tube was put into the FMR cavity, where the suspension was exposed to a magnetic field of 7 kOe (560 A/m) and frozen upon cooling to 200 K in the presence of the field (24).

FMR spectra simulation

For a quantitative analysis, FMR data obtained from bulk samples and samples with aligned MTB were compared to simulate signals. In the bulk samples, which contain a great number of bacteria, the axes of the magnetosome chains are generally randomly distributed and there are dipoles pointing in all possible directions. In this configuration the FMR spectra of MTB exhibit no angular dependence and present typical features consisting of two low-field peaks and a strong high-field peak (21). Charilaou et al. (23) presented a theoretical approach for bulk samples, which takes into account the magnetocrystalline field, H_{cub}, originating from the arrangement of the atoms in the crystal structure of each magnetite particle and the uniaxial field, H_{uni}, due to the particle interaction in chain configuration, also denoted as interaction-induced shape anisotropy. With this approach, FMR spectra of MTB can be simulated and anisotropy parameters can be quantitatively extracted by fitting the experimental data.

The calculation of the resonance fields was performed by solving the resonance equation

$$(\omega/\gamma)^2 = H_{eff}, \tag{1}$$

where ω is the microwave frequency, γ is the gyromagnetic ratio, and H_{eff} is the effective magnetic field inside the magnetic particles, which consists of the external field, H_{ex}, the dipole field, H_{uni}, and the anisotropy field, H_{cub}. When Eq. 1 is satisfied, then $H_{eff} = H_{res}$.

The contributions to the total energy density, F_{tot}, are 1) the Zeeman energy (due to the external field),

$$F_z = -\vec{M} \times \vec{H}_{ex}; \tag{2}$$

2) the magnetostatic self-energy (dipolar fields),

$$F_{\text{dip}} = 2\pi N_{\text{eff}} M^2 \sin^2\theta, \quad (3)$$

where N_{eff} is the effective demagnetizing tensor and θ is the polar angle, i.e., the angle between the external magnetic field and the axis of the chain; and 3) the magnetocrystalline contribution,

$$H_{\text{cub}} = K_1 \sin^2\theta - \frac{K_1}{8}(\cos 4\varphi + 7)\sin^4\theta, \quad (4)$$

where K_1 is the first-order anisotropy constant of magnetite (10^5 erg/cm^3 or 10 kJ/m^3 at room temperature) and φ is the azimuth angle, i.e., the angle between the external field and the crystalline (100) axis. Given the above, we define the uniaxial and cubic anisotropy fields as $H_{\text{uni}} = 4\pi N_{\text{eff}} M$ and $H_{\text{cub}} = K_1/M$, respectively.

The calculation of the resonance fields, H_{res}, at each set of field angles (θ, φ) is done at equilibrium from the derivatives of the energy density (29,30). Then, using the values of $H_{\text{res}}(\theta, \varphi)$ we generate FMR signals in the form of Gaussian derivative curves with a linewidth of 250 Oe (20 kA/m) for each set of (θ, φ). For a bulk sample, the FMR spectrum corresponds to the superposition of all possible orientations of the magnetic field with respect to the particle chain, so we add all the FMR signals, weighed with the spatial distribution probability $p(\theta) = \sin\theta/4\pi$ and convolute with a certain broadening. For a more detailed explanation of the simulation process, see Charilaou et al. (23).

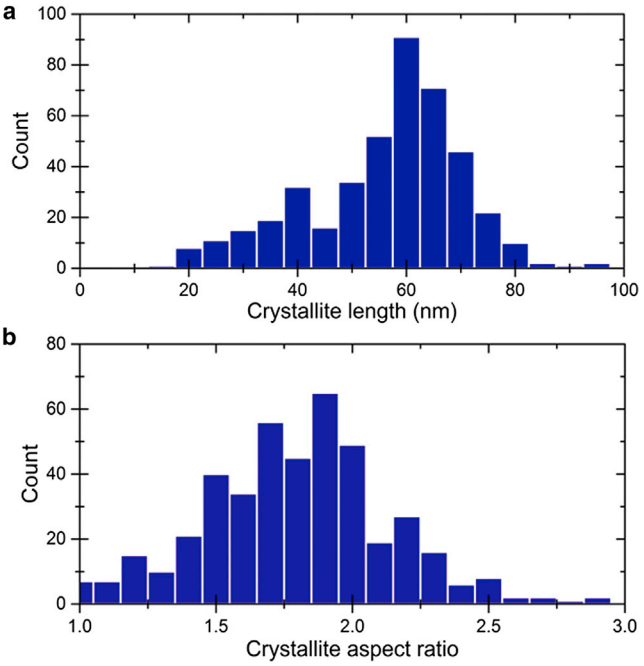

FIGURE 2 Distribution of crystallite length (*a*) and crystallite aspect ratio (length/width) (*b*) of intracellular magnetite particles.

RESULTS AND DISCUSSION

TEM micrographs of the cultured RS-1 strain show intracellular bullet-shaped magnetite nanoparticles assembled in chains (Fig. 1). Extracellular iron oxide particles as reported by Pósfai et al. (15) are not observed. In our sample, the chains generally consist of <10 magnetosomes, but a bacterial cell can contain more than one of these assemblies. The statistical analysis of the magnetite particle size exhibits an average length of 53.8 ± 14.2 nm (Fig. 2 *a*). This value is significantly larger than 30 nm, the theoretical threshold for noninteracting stable single-domain magnetite (31). The distribution of the crystal lengths reveals that a minor number of particles are between 20 and 30 nm, a size range in which magnetite is generally in a superparamagnetic state. Dipolar interaction as it occurs in chain configuration stabilizes the magnetic moments and therefore, the magnetic particles in the RS-1 cells are in a stable single-domain state (32). The smaller particles generally occur at the ends of the chains (Fig. 1). Considering the RS-1 growth series by Byrne (27) these more equidimensional particles may represent an earlier state during the formation of magnetosome magnetite. The bullet-shaped magnetic particles display some variation in their morphology and an average shape factor (length/width) of 1.77 ± 0.4 (Fig. 2 *b*). The morphological properties and the configuration in the cell of our cultured RS-1 strain are similar to those reported for the same strain (15,27). Because high-resolution TEM provided direct evidence that bullet-shaped nanocrystals in the RS-1 strain are typically elongated along (100), which is the magnetic hard axis of the magnetite (15), it can be assumed that in the cells of our sample, the magnetosomes are also aligned along their hard axes.

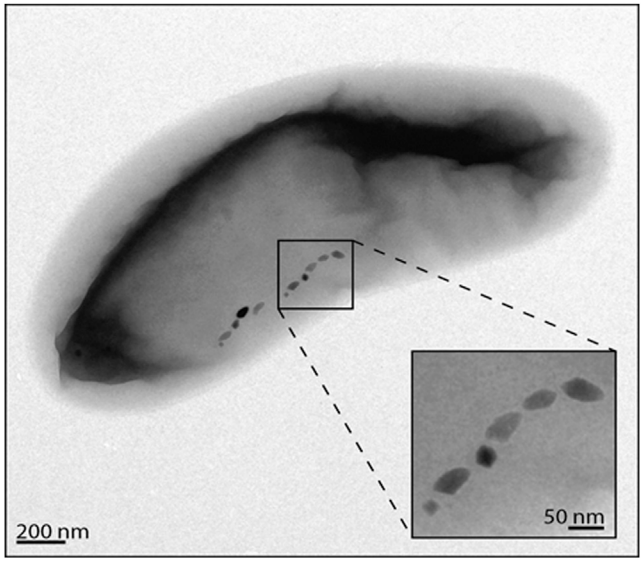

FIGURE 1 TEM image of a single bacterium showing magnetite nanocrystals aligned along the long axis of the cell.

Fig. 3 shows the comparison between the FMR spectra of two samples of the RS-1 strain differing in the configurations of their magnetosome chains. In the oriented MTB sample, the magnetosome chains are aligned (Fig. 3 *a*, *inset*), whereas in the bulk sample they are randomly distributed (Fig. 3 *b*, *inset*). Along the easy axis of the magnetization in the oriented sample (Fig. 3 *a*), i.e., along the axis of

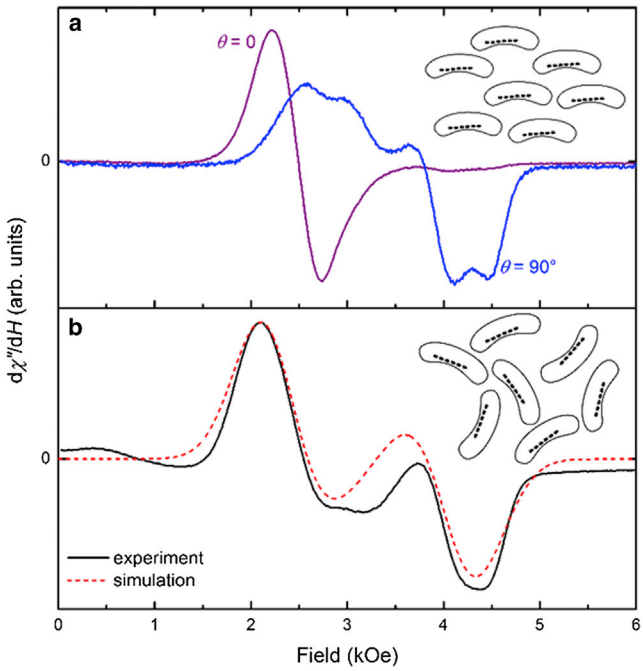

FIGURE 3 FMR spectra yielded from RS-1 strain in two configurations at $T = 200$ K. (*a*) Measured spectra of aligned MTB cells with the external field parallel (*purple*) and perpendicular (*blue*) to the magnetic dipole of the cell. (*b*) Spectrum of a sample with randomly oriented cells, as indicated by the cartoon. The spectrum of the random sample was simulated using the model discussed in Vonsovskii (18).

the magnetosome chain ($\theta = 0$), the FMR spectrum has a symmetric Lorentzian derivative shape, and the resonance field (H_{res}) is ~2.5 kOe (200 kA/m). When the external field is perpendicular to the magnetosome chains ($\theta = 90°$), the FMR spectrum is shifted to a field of ~4 kOe (320 kA/m), and the shape of the signal is very broad and highly asymmetric. This asymmetry comes from additional contributions of the magnetocrystalline anisotropy that become evident at $\theta = 90°$, as discussed below.

The FMR signal obtained from the sample with randomly distributed MTB represents a spectral superposition from magnetosome chains in a range of θ between 0 and 90°. Comparing the spectra in Fig. 3, *a* and *b*, the low-field peak of the random sample coincides with the FMR spectrum of the oriented sample at $\theta = 0$, and in a similar way, the high-field feature of the random sample coincides with the FMR spectrum of the oriented sample perpendicular to the magnetic field. This indicates that the dominant features of the FMR spectrum in the random sample originate from magnetosome chains oriented parallel and perpendicular to the magnetic field, and that the features between the low- and high-field peaks arise from contributions of intermediate orientations. It is worth noting that the FMR spectra show no indication of superparamagnetic particles, characterized by narrow signals at $H_{res} \approx 3.4$ kOe (270 kA/m), or of hematite, which generally shows broad signals (23,33), and this is in good agreement with the microscopic results.

To quantify the magnetic anisotropy of the RS-1 strain, we recorded FMR spectra of the oriented sample at different angles, from 0 to 180°, and plotted the resonance field, H_{res}, as a function of the angle θ between the magnetic field and the magnetic dipole of the chains. Fig. 4 *a* shows the angular dependence of the resonance field, as extracted from the experiments (open circles), and a fit to the data, obtained by simulating H_{res} using H_{uni} and H_{cub} as input. The calculation provides a very good fit to the data, allowing the extraction of the anisotropy fields with a high degree of precision. At $T = 200$ K, we find an effective uniaxial anisotropy field of 1000 ± 10 Oe (80 kA/m), and a cubic magnetocrystalline anisotropy field of -150 ± 5 Oe (12 kA/m). The magnetocrystalline field is in very good agreement with known values of magnetite crystals at this temperature, which are slightly lower than those at room temperature (34,35).

From these values of the anisotropy fields, we can plot the two components of anisotropy as a function of the angle θ to

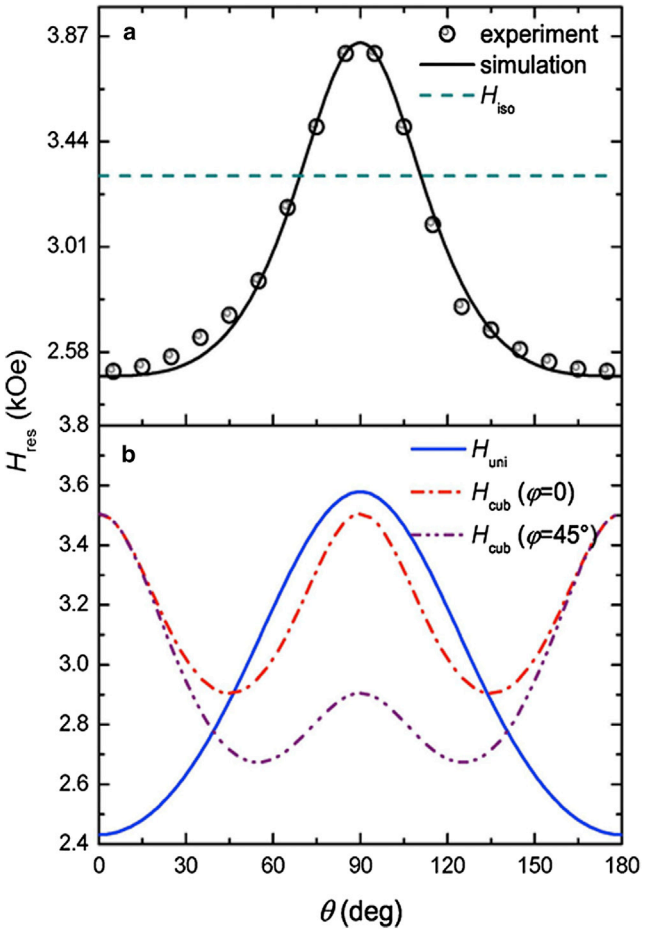

FIGURE 4 Angular dependence of the resonance field of the oriented MTB sample. (*a*) Open circles correspond to experimental results and the solid line corresponds to a fit calculated using a cubic anisotropy field of $H_{cub} = -160$ Oe (12.7 kA/m) and a uniaxial field of $H_{uni} = 1000$ Oe (80 kA/m). The horizontal dashed line indicates the isotropic resonance field, H_{iso}. (*b*) The blue line and the dash-dotted lines show the individual contributions of H_{cub} and H_{uni}, respectively.

compare their relative contributions to the total anisotropy (see Fig. 4 *b*). The uniaxial field, H_{uni}, has a minimum at $\theta = 0$ and 180°, i.e., parallel to the magnetosome chains, and a maximum at $\theta = 90°$. The magnetocrystalline field, H_{cub}, has a maximum for chains perpendicular to the magnetic field too, but it also has maxima along the chain axis, whereas the minima lie at $\theta = 45°$. To take into account the three dimensions of the crystalline symmetry, we also consider the azimuth angle, and as seen in Fig. 4, the azimuthal orientation of a magnetite particle can have a drastic effect on the resonance field at $\theta = 90°$. For $\varphi = 0$, the value of H_{res} for $\theta = 90°$ is exactly the same as for $\theta = 0$. However, when $\varphi = 45°$, H_{res} for $\theta = 90°$ is much lower than that for $\theta = 0$, i.e., this is an intermediate axis of the magnetization. The resonance field of a magnetosome chain can therefore be strongly affected not only by the angle between the magnetic field and the chain, as was the case for the previously studied MTB (see, e.g., Charilaou and colleagues (23,24)) but by the azimuthal angle between the magnetic field and the easy (111) axis of magnetite. This also explains the broad and structured FMR spectrum at $\theta = 90°$ in the oriented sample, which is caused by different magnetocrystalline contributions that superimpose to generate a broad FMR response.

Given the above, we can visualize the anisotropy properties of the RS-1 strain using the values of the resonance field to understand the effect of the chains being aligned along (100) and not along (111) and to compare the magnetic performance of RS-1 against those of MTB strains in which the magnetosomes are aligned in the chain along their (111) crystallographic directions. Fig. 5 shows a comparison of the anisotropy of the RS-1 strain with that previously reported for the *M. gryphiswaldense* (strain MRS-1), which exhibited the same anisotropy fields, i.e., $H_{uni} = 1000$ Oe (80 kA/m) and $H_{cub} = -150$ Oe (12 kA/m) (19).

The color map shows the resonance field at each set of angles (φ,θ). For RS-1 (Fig. 5 *a*), the fourfold symmetry around the (100) axis of magnetite is clearly apparent, and it is superimposed by the uniaxial anisotropy. In *M. gryphiswaldense* (Fig. 5 *b*), the three-fold symmetry of the (111) axis is evident, and the uniaxial character is more pronounced, since the magnetocrystalline easy axis of (111) coincides with the chain axis.

The organization of magnetite particles along the (100) hard axis is energetically unfavorable and leads to a magnetization that departs from equilibrium, conferring a disadvantage on RS-1 relative to strains of the *α-proteobacteria*, since it is unable to generate a stable dipole. However, this can be outweighed by the formation of elongated particles, which have predominant shape anisotropy. The uniaxial anisotropy due to elongation along (100) is then in competition with the magnetocrystalline easy axis, and the equilibrium magnetization departs from the (111) direction toward the axis of elongation. Magnetic modeling showed that with an aspect ratio >1.25 the (100) axis of elongation

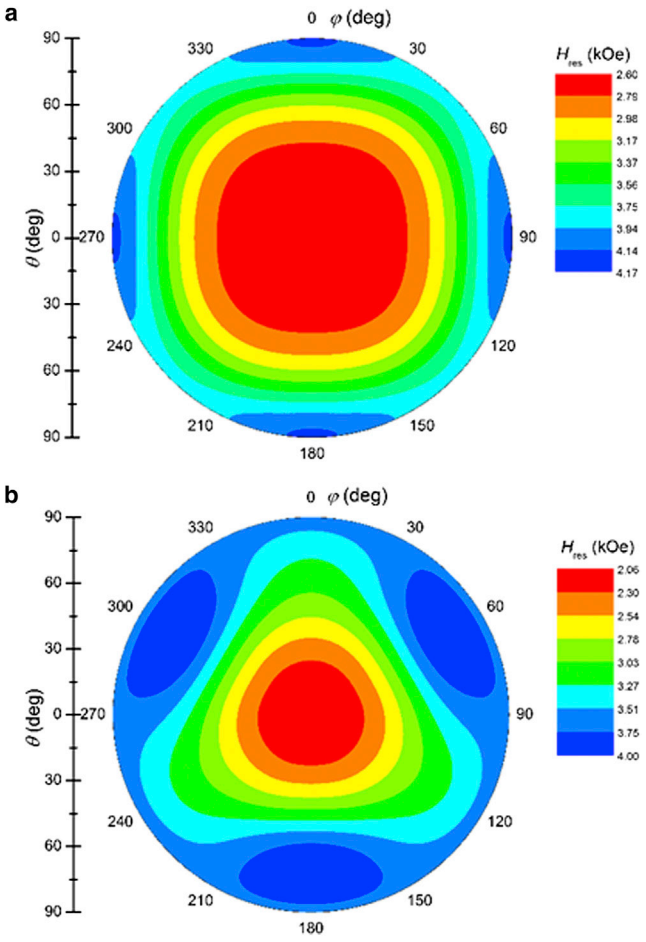

FIGURE 5 Anisotropy map of MTB, simulated using parameters extracted from FMR experiments. (*a*) Anisotropy of RS-1 MTB (as seen by facing the long axis of the chain). (*b*) Typical symmetry of most MTB strains in the α-proteobacteria class, such as *M. gryphiswaldense*. The difference between the RS-1 strain and MTB affiliated with the α-proteobacteria is that the cubic magnetocrystalline symmetry does not coincide with the uniaxial direction of the dipole field in the nanoparticle chain.

becomes the effective easy axis (16). The majority of the magnetosomes in our sample have an average aspect ratio of 1.8, which is much higher than 1.25 (Fig. 2 *b*). This implies that H_{uni} results from magnetic moments aligned parallel to the longitudinal axis of the cell, similar to those in MTB strains of the α-proteobacteria. This is supported if one compares the ratio of the anisotropy fields H_{uni} and H_{cub} as a proxy for the dipole in MTB. In this study, a ratio of $|H_{uni}/H_{cub}| = 6.6$ has been determined for aligned RS-1 strain at $T = 200$ K and a similar ratio, $|H_{uni}/H_{cub}| = 6.4$, for *M. gryphiswaldense* at the same temperature (24). The nearly identical value suggests that the uniaxiality of MTB with intracellular magnetite particles does not vary strongly among different Proteobacteria classes. Recently published FMR spectra indicate that uncultured coccoid MTB of the α-proteobacteria class, with unusually large magnetosome magnetite arranged in chains along (111), have a markedly enhanced H_{uni} compared to

M. gryphiswaldense (36,37). Such a size effect, however, is not critical for comparison of the RS-1 and MSR-1 strains because their particle sizes are in a similar range.

Growth series of the *M. gryphiswaldense* strain MSR-1 and *Desulfovibrio magneticus sp*. strain RS-1 have shown that these two MTB strains follow different strategies to build up cellular magnetic dipoles (9,23). In *M. gryphiswaldense*, magnetite nucleates and grows in widely spaced organelles along cytoskeletal filaments at which the magnetic nanoparticles are noninteracting. The subsequent movement of the organelles along the filament brings the magnetite nanoparticles together so that dipole interactions generate uniaxiality (9,25,38). This docking enhances the stability of the magnetosome chains. It is worth noting that a slightly different mechanism has been found for the α-proteobacteria *M. magneticum* AMB-1, where the magnetite nanoparticles are precipitated in organelles with a close spacing (8). During the growth of the MTB, the nanoparticles reach the size where dipolar interactions between them are established and chain assembly occurs with a pronounced uniaxiality. In both cases, key proteins have been deciphered that regulate the formation of magnetosome chains and in turn the cellular magnetic dipole (8,9).

By contrast, for the RS-1 strain, no membrane sheath has been found associated with the magnetite nanoparticles forming the cellular dipole (27). Moreover, the growth series by Byrne et al. (27) provided evidence that before the formation of magnetite magnetosomes, RS-1 biomineralizes amorphous iron-rich granules in organelles. The two iron phases are likely formed through separate cellular processes (27). The precipitation of the amorphous phase in organelles suggests a cellular process triggered by specific proteins. The formation of the bullet-shaped magnetite nanoparticles without magnetosome membranes that are assembled in chain-like configurations is presumably assisted by non-biologically-controlled processes. The more variable shape and assembly of magnetic particles in RS-1 compared to those in species of α-proteobacteria (e.g., *M. gryphiswaldense*) could be a hint that the formation of chain-like assemblies in RS-1 is critically affected by self-organized processes of the magnetite particles stabilized by the cytoplasm rather than by processes solely controlled by magnetosome-related genes and proteins. In any case, the complex formation mechanisms of the magnetite chains in MTB are explained by comparing the anisotropy maps yielded from MRS-1 and RS-1 strains, which show that in RS-1, the individual nanoparticles forming chain-like assemblies have a higher degree of orientational flexibility (cf. Fig. 5, *a* and *b*, *red area*) The higher flexibility involves a weakening of the dipole of the chain-like assemblies. Because the bullet shape is considered to be the first morphology of magnetite nano-particles biomineralized by MTB (4), this trade-off of efficiency versus flexibility seems to be shifted toward efficiency during the evolutionary development of MTB.

CONCLUSIONS

In summary, the quantitative FMR analysis of the MTB *Desulfovibrio magneticus sp.* strain RS-1 experimentally confirms previous microscopic observations that the intracellular bullet-shaped magnetite nanoparticles are aligned along their magnetocrystalline (100) hard axis. The alignment of the magnetic nanoparticles in the cell along (100), which is energetically less favorable, creates a mixed anisotropy system with the contribution of the (111) magnetocrystalline easy axis of magnetization. Quantitative comparison with the anisotropy properties of *M. gryphiswaldense* shows that the configuration of the magnetite nanoparticles in RS-1 has no critical effect on the cellular dipole moment due to the pronounced uniaxiality of the individual particles. From a physical point of view, the balance between elongation and alignment of the intracellular nanoparticles as found in RS-1 could be a reason for the persistence of the bullet-shaped magnetite morphology during the evolution of magnetotaxis in MTB.

REFERENCES

1. Blakemore, R. 1975. Magnetotactic bacteria. *Science.* 190:377–379.
2. Blakemore, R. P., R. B. Frankel, and A. J. Kakmijn. 1980. South-seeking magnetotactic bacteria in the southern hemisphere. *Nature.* 286:384–385.
3. Bazylinski, D. A., and R. B. Frankel. 2004. Magnetosome formation in prokaryotes. *Nat. Rev. Microbiol.* 2:217–230.
4. Lefèvre, C. T., D. Trubitsyn, …, D. A. Bazylinski. 2013. Monophyletic origin of magnetotaxis and the first magnetosomes. *Environ. Microbiol.* 15:2267–2274.
5. Devouard, B., M. Pósfai, …, P. R. Buseck. 1998. Magnetite from magnetotactic bacteria: size distribution and twinning. *Am. Mineral.* 83:1387–1398.
6. Dunin-Borkowski, R. E., M. R. McCartney, …, P. R. Buseck. 1998. Magnetic microstructure of magnetotactic bacteria by electron holography. *Science.* 282:1868–1870.
7. Komeili, A., H. Vali, …, D. K. Newman. 2004. Magnetosome vesicles are present before magnetite formation, and MamA is required for their activation. *Proc. Natl. Acad. Sci. USA.* 101:3839–3844.
8. Komeili, A., Z. Li, …, G. J. Jensen. 2006. Magnetosomes are cell membrane invaginations organized by the actin-like protein MamK. *Science.* 311:242–245.
9. Scheffel, A., M. Gruska, …, D. Schüler. 2006. An acidic protein aligns magnetosomes along a filamentous structure in magnetotactic bacteria. *Nature.* 440:110–114.
10. Murat, D., A. Quinlan, …, A. Komeili. 2010. Comprehensive genetic dissection of the magnetosome gene island reveals the step-wise assembly of a prokaryotic organelle. *Proc. Natl. Acad. Sci. USA.* 107:5593–5598.
11. Lohße, A., S. Borg, …, D. Schüler. 2014. Genetic dissection of the *mamAB* and *mms6* operons reveals a gene set essential for magnetosome biogenesis in *Magnetospirillum gryphiswaldense*. *J. Bacteriol.* 196:2658–2669.
12. Pósfai, M., C. T. Lefèvre, …, R. B. Frankel. 2013. Phylogenetic significance of composition and crystal morphology of magnetosome minerals. *Front Microbiol.* 4:350–368.
13. Faivre, D., and D. Schüler. 2008. Magnetotactic bacteria and magnetosomes. *Chem. Rev.* 108:4875–4898.

14. Jimenez-Lopez, C., C. S. Romanek, and D. A. Bazylinski. 2010. Magnetite as a prokaryote biomarker: a review. *J. Geophys. Res.* 115:G00G03. http://dx.doi.org/10.1029/2009JG001152.

15. Pósfai, M., B. M. Moskowitz, …, R. B. Frankel. 2006. Properties of intracelllular magnetite crystals produced by *Desulfovibro magneticus* strain RS-1. *Earth Planet. Sci. Lett.* 249:444–455.

16. Körnig, A., M. Winklhofer, …, D. Faivre. 2014. Magnetite crystal orientation in magnetosome chains. *Adv. Funct. Mater.* 24:3926–3932. http://dx.doi.org/10.1002/adfm201303737.

17. Lefèvre, C. T., M. Pósfai, …, D. A. Bazylinski. 2011. Morphological features of elongated-anisotropic magnetosome crystals in magnetotactic bacteria of the *Nitrospirae* phylum and the *Deltaproteobacteria* class. *Earth Planet. Sci. Lett.* 312:194–200.

18. Vonsovskii, S. V. 1966. Ferromagnetic Resonance: The Phenomenon of Resonant Absorption of a High-Frequency Magnetic Field in Ferromagnetic Substances. Pergamon Press, Oxford, United Kingdom.

19. Weiss, B. P., S. S. Kim, …, A. Komeili. 2004. Ferromagnetic resonance and low-temperature magnetic test for biogenic magnetite. *Earth Planet. Sci. Lett.* 224:73–89.

20. Kopp, R. E., C. Z. Nash, …, J. L. Kirschvink. 2006. Ferromagnetic resonance spectroscopy for assessment of magnetic anisotropy and magnetostatic interactions: a case study of mutant magnetotactic bacteria. *J. Geophys. Res.* 111:B12S25. http://dx.doi.org/10.1029/2006JB004529.

21. Fischer, H., G. Mastrogiacomo, …, A. U. Gehring. 2008. Ferromagnetic resonance and magnetic characteristics of intact magnetosome chains in *Magnetospirillum gryphiswaldense*. *Earth Planet. Sci. Lett.* 270:200–208.

22. Mastrogiacomo, G., H. Fischer, …, A. U. Gehring. 2010. Ferromagnetic resonance spectroscopic response of magnetite chains in a biological matrix. *J. Magn. Magn. Mater.* 322:661–663.

23. Charilaou, M., M. Winklhofer, and A. U. Gehring. 2011. Simulation of ferromagnetic resonance spectra of linear chains of magnetite nanocrystals. *J. Appl. Phys.* 109:093903.

24. Charilaou, M., J. Kind, …, A. U. Gehring. 2014. Magnetic anisotropy of non-interacting collinear nanocrystal-chains. *Appl. Phys. Lett.* 104:112406.

25. Charilaou, M., K. K. Sahu, …, A. U. Gehring. 2011. Evolution of magnetic anisotropy and thermal stability during nanocrystal chain growth. *Appl. Phys. Lett.* 99:182504.

26. Sakaguchi, T., J. G. Burgess, and T. Matsunga. 1993. Magnetite formation by a sulphate-reducing bacterium. *Nature.* 365:47–49.

27. Byrne, M. E., D. A. Ball, …, A. Komeili. 2010. *Desulfovibrio magneticus* RS-1 contains an iron- and phosphorus-rich organelle distinct from its bullet-shaped magnetosomes. *Proc. Natl. Acad. Sci. USA.* 107:12263–12268.

28. Gehring, A. U., J. Kind, …, I. García-Rubio. 2011. The detection of magnetotactic bacteria and magnetofossils by means of magnetic anisotropy. *Earth Planet. Sci. Lett.* 309:113–117.

29. Smit, J., and H. G. Beljers. 1955. Ferromagnetic resonance absorption in $BaFe_{12}O_{19}$, a highly anisotropic crystal. *Philips Res. Rep.* 10: 113–130.

30. Baselgia, L., M. Warden, …, M. Marysko. 1988. Derivation of the resonance frequency from the free energy of ferromagnets. *Phys. Rev. B Condens. Matter.* 38:2237–2242.

31. Butler, R. F., and S. K. Banerjee. 1975. Theoretical single-domain grain size range in magnetite and titanomagnetite. *J. Geophys. Res.* 80:4049–4058.

32. Muxworthy, A. R., and W. Williams. 2009. Critical superparamagnetic/single-domain grain sizes in interacting magnetite particles: implications for magnetosome crystals. *J. R. Soc. Interface.* 6:1207–1212.

33. Gehring, A. U., and A. M. Hofmeister. 1994. The transformation of lepidocrocite during heating: A magnetic and spectroscopic study. *Clays Clay Miner.* 42:409–415.

34. Abe, K., Y. Y. Miyamoto, and S. Chikazumi. 1976. Magnetocrystalline anisotropy of low temperature phase of magnetite. *J. Phys. Soc. Jpn.* 41:1894–1902.

35. Bickford, L. R. 1950. Ferromagnetic absorption in magnetite single crystal. *Phys. Rev.* 78:449–457.

36. Abraçado, L. G., E. Wajnberg, …, M. Farina. 2014. Ferromagnetic resonance of intact cells and isolated crystals from cultured and uncultured magnetite-producing magnetotactic bacteria. *Phys. Biol.* 11:036006. http://dx.doi.org/10.1088/1478–3975/11/3/036006.

37. Spring, S., U. Lins, …, M. Farina. 1998. Phylogenetic affiliation and ultrastructure of uncultured magnetic bacteria with unusually large magnetosomes. *Arch. Microbiol.* 169:136–147.

38. Faivre, D., A. Fischer, …, A. U. Gehring. 2010. Development of cellular magnetic dipoles in magnetotactic bacteria. *Biophys. J.* 99:1268–1273.